Proceedings of the 3rd Marine Energy Technology Symposium
METS2015
April 27-29, 2015, Washington, DC

HYDRODYNAMIC OPTIMIZATION OF CROSS-FLOW TURBINES WITH LARGE CHORD TO RADIUS RATIOS

Benjamin Strom*
Northwest National Marine
Renewable Energy Center
University of Washington
Seattle, WA, USA

Brian Polagye
Northwest National Marine
Renewable Energy Center
University of Washington
Seattle, WA, USA

Steve Brunton
Northwest National Marine
Renewable Energy Center
University of Washington
Seattle, WA, USA

INTRODUCTION

Cross-flow turbines present several advantages over axial flow types for power generation from moving water. First, the rectangular form factor is well suited to take advantage of the hydrokinetic energy often concentrated in shallow channels. This form factor presents an opportunity to construct arrays with high blockage (ratio of swept area to channel cross-sectional area), potentially increasing energy extraction beyond the Betz limit for unconfined flows [1]. Second, in bidirectional tidal flows, yaw control is unnecessary. Thirdly, for high-solidity cross-flow turbines, the maximum blade speed is typically lower than axial flow turbines, reducing the risk of cavitation, acoustic pollution, and harmful interactions between devices and marine fauna.

Though the foil kinematics in a cross-flow turbine exhibit just one degree of freedom, the resulting fluid dynamics are complex and highly dependent on turbine geometric parameters [2], [3]. In this study we examine the performance implications of altering the blade pitch angle and the number of blades on cross-flow turbines.

Geometric Parameters of Cross-Flow Turbines

The design parameters responsible for the geometry of a cross-flow turbine are given in Table 1. From these, the following non-dimensional quantities are derived: turbine aspect ratio

$$AR = \frac{2R}{L}, \tag{1}$$

TABLE 1: TURBINE GEOMETRY PARAMETERS

R	Turbine radius
L	Turbine span (height)
c	Blade chord
N	Blade count
α_p	Preset blade pitch angle
β	Blade helix angle
-	Blade profile
-	Blade end condition

solidity

$$\sigma = \frac{Nc}{2\pi R}, \tag{2}$$

and chord to radius ratio

$$R_c = \frac{c}{R}. \tag{3}$$

Cross-Flow Turbine Hydrodynamics

The hydrodynamics of cross-flow turbines can be reduced to three semi-interdependent categories: induced flow, three dimensional effects (flow variation in the spanwise direction), and individual foil hydrodynamics. Induced flow includes axial and angular induction, internal wake deficit, and the generation of coherent structures. Three dimensional effects include the effect of the end condition of the blades (free vs. end plates), the turbine aspect ratio, and the hydrodynamic effect of helical blades. Individual foil hydrodynamics, the focus of this paper, include the

*Corresponding Author: strombw@uw.edu

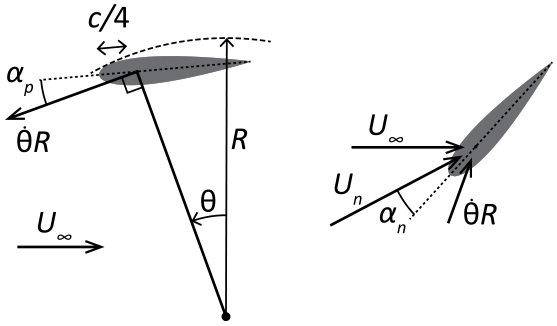

FIGURE 1: PRESET BLADE PITCH, α_p (LEFT) AND NOMINAL ANGLE OF ATTACK, α_n (RIGHT). THE AZIMUTHAL BLADE POSITION IS DENOTED BY θ ($\theta = 0$ WHEN $\dot{\theta}R$ POINTS UPSTREAM). THE FREE STREAM VELOCITY IS U_∞ AND THE NOMINAL VELOCITY IS U_n.

variation of the effective angle of attack and nominal velocity with angular blade position, as well as dynamic stall.

Preset Pitch Hydrodynamics

Figure 1 (left) visualizes the preset pitch angle, given as the rotation angle of the foil about the quarter chord with respect to the line tangent to the rotation direction. As for angle of attack, we define a positive pitch angle as the leading edge rotated away from the turbine axis. Assuming a constant free stream velocity, no induced velocity, and a constant rotation rate, the nominal (effective) angle of attack experienced by the foil (Fig. 1, right) is given by

$$\alpha_n = \tan^{-1}\left(\frac{\dot{\theta}R\sin(\alpha_p)+U_\infty\sin(\alpha_p-\theta)}{\dot{\theta}R\cos(\alpha_p)+U_\infty\cos(\alpha_p-\theta)}\right) \tag{4}$$

The effect of adding a preset pitch angle on the nominal angle of attack is shown in fig. 2 for various tip speed ratios, given by

$$\lambda = \frac{\omega R}{U_\infty} \tag{5}$$

where ω is the turbine rotation rate and U_∞ is the free stream velocity.

High Chord to Radius Hydrodynamics

Previous experiments indicate that the optimal tip speed ratio for a vertical axis wind turbine is inversely related to R_c [3], [4], [5]. The Glauert criterion suggests a lower maximum possible efficiency for axial flow turbines with lower tip speed ratios [6]. For this reason, vertical axis wind turbines have evolved to operate at high tips speed ratios, achievable by using low solidity (<5%) and chord to radius ratios. However, for hydrokinetic applications, the potential decrease in energy conversion efficiency with increase in R_c is offset by several advantages. First, a lower tip speed ratio reduces risk of cavitation (especially important for near-surface devices, such as those in high blockage arrays), decreases vibration frequency and magnitude, and may reduce risk to marine animals. In addition, the larger relative chord allows for more robust blades.

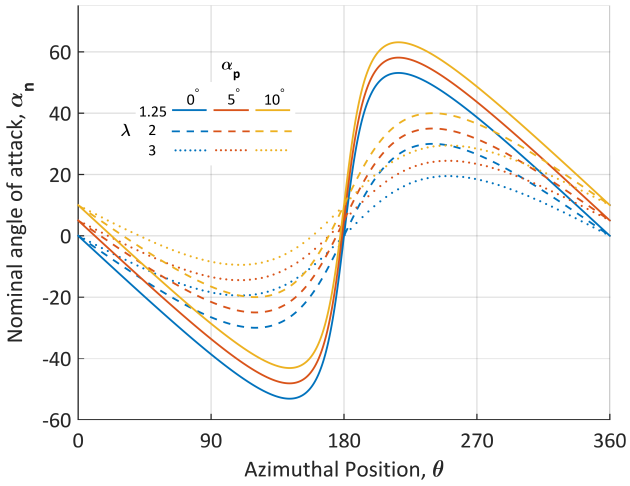

FIGURE 2: THE EFFECT OF PRESET BLADE PITCH (α_p) ON NOMINAL ANGLE OF ATTACK (AT THE MOUNT POINT) FOR VARIOUS TIP SPEED RATIOS (λ). THIS ASSUMES NO INDUCED VELOCITY.

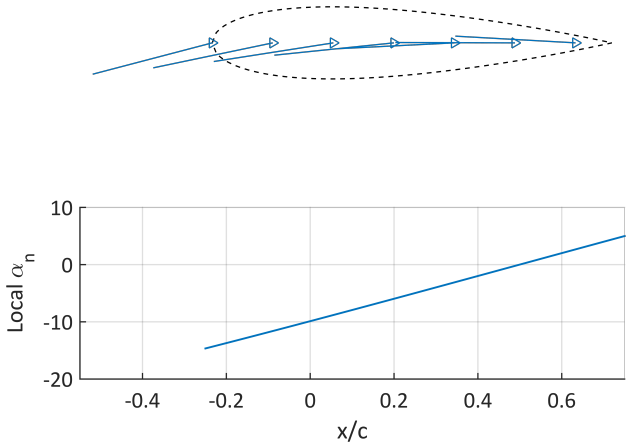

FIGURE 3: LOCAL NOMINAL ANGLE OF ATTACK VARIATION ALONG CHORD LENGTH. HERE $\theta = 30°$, $\alpha_p = 0$, $\lambda = 2$, and $R_c = 0.5$. $x = 0$ IS AT THE MOUNT POINT, $c/4$.

For turbines with a large chord to radius ratio, the angle of attack can vary significantly along the chord length of the blade (Fig. 3). The net fluid dynamic result of a chord-wise variation in local angle of attack is the same as a cambered blade in rectilinear flow. As in [7], we refer to this effect as virtual camber.

Previous studies suggest that the importance of preset pitch

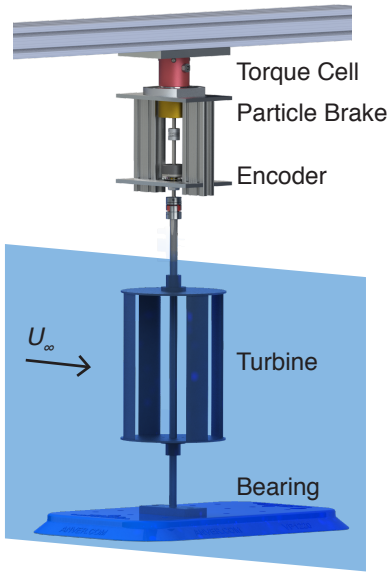

FIGURE 4: EXPERIMENTAL SETUP DIAGRAM WITH A FOUR-BLADED TURBINE.

(α_p in Fig. 1) increases with solidity or chord to radius ratio [8] [9].

METHODS

Due the wake-foil interaction and other hydrodynamic complexities described previously, numerical or analytic simulation of cross-flow turbines with high R_c is difficult. For this reason, we chose to pursue the optimization of turbine parameters experimentally.

Experimental Turbine

The cross flow turbine used in this study consisted of two circular endplates mounted on a 1.3 cm shaft. Straight blades were mounted at the periphery of the end plates at various preset pitch angles, such that the maximum turbine radius remained constant at 8.6 cm. A symmetric NACA0018 blade profile with a 4.05 cm chord was used. One, two, and four bladed turbines were tested with respective solidities of $\sigma = 0.075$, 0.15, and 0.3. The turbine aspect ratio was 1.36. NACA4512 foils were used to study the effects of blade camber. This foil was chosen for its favorable lift to drag ratio at the predicted Reynolds number and maximum nominal angle of attack.

Flume

Experiments were performed in a water flume with a test section measuring 75 cm wide by 48 cm deep (while running). The resulting blockage ratio (the turbine swept area to the flume cross sectional area) was 0.11. Previous studies suggest blockage values over about 0.05 will inflate turbine performance measurements compared to performance in unconfined flow [10] [11]. The free stream velocity was measured at $10R$ upstream from the turbine using an acoustic Doppler velocimeter at a sample rate of 100 Hz. The turbulent intensity of the incoming flow was 1.8%. The blade chord Reynolds number (neglecting the turbine angular velocity and induction), given by

$$Re_c = \frac{U_\infty c}{\nu}, \tag{6}$$

was 3.2×10^4. Prior experiments with a helical cross-flow turbine demonstrated Reynolds number independent performance above $Re_c = 4.2 \times 10^4$ and a significant decrease in efficiency below this. However, the maximum flow velocity of the flume for these experiments (0.7 m/s) prevented operation above this threshold.

Performance Characterization Procedure

A resistive torque was applied to the turbine drive shaft via a electromagnetic particle brake. Keeping the free stream velocity at a constant 0.7 m/s, the torque was incremented from a no-load condition until turbine stall occurred. At each resistive torque setting, the particle brake torque (τ) was measured using a torque cell at an acquisition rate of 200 Hz (this includes both the hydrodynamic and acceleration forces, with the latter integrating to zero over one cycle at steady state operation). The turbine azimuthal position (θ) was measured by a 500 count per revolution optical encoder.

Each mean oppositional torque setting yielded a mean tip speed ratio. Turbine performance curves were generated by comparing the mean tip speed ratio to the power coefficient, calculated as

$$C_p = \frac{\dot{\theta}\tau}{\rho U_\infty^3 RL}, \tag{7}$$

where the denominator is the kinetic power available in the area swept by the turbine blades.

RESULTS AND DISCUSSION

Blade Profile

Figure 5 shows a comparison of the performance of symmetric and cambered foils. Virtual camber induced by the curvilinear nature of the flow experienced by the foil increases with R_c (because there is more chord over which to vary the local angle of attack) and decreases with increased λ (because the effective velocity parallel to the chord is larger, reducing changes in local angle of attack). As λ is small and R_c is large, significant virtual camber is present at some azimuthal positions. Figure 6 shows the virtual camber for the NACA0018 foil given the same parameters as the performance curves in Fig. 5.

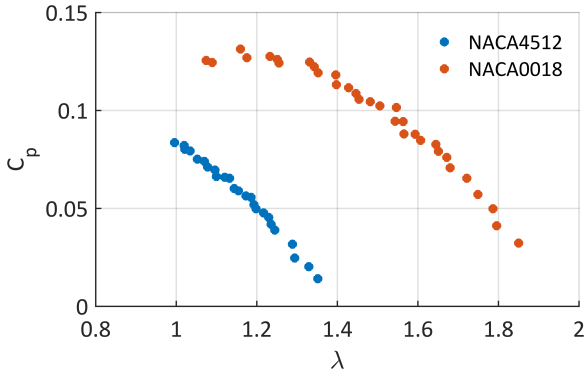

FIGURE 5: PERFORMANCE CURVE COMPARISON OF CAMBERED AND UNCAMBERED FOILS. HERE $N = 4$, and $\alpha_p = 6°$. THE CAMBER OF THE NACA4512 FACES OUTWARD.

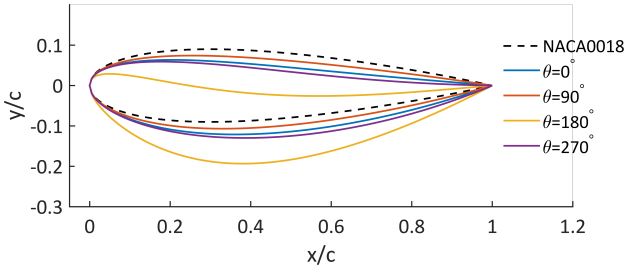

FIGURE 6: VIRTUAL CAMBER DUE TO FLOW CURVATURE, CALCULATED AS GIVEN IN [7] FOR VARIOUS AZIMUTHAL BLADE POSITIONS, θ. HERE $\lambda = 1.5$ AND $R_c = 0.47$. NEGLECTS INDUCTION AND WAKE EFFECTS.

This is likely responsible for the failure of the NACA4512 foil to outperform the symmetric foil. First, the symmetric foil is already exhibiting lift and drag dynamics of a cambered foil. Second, the virtual camber of the already cambered NACA4512 is likely so extreme at some points in the cycle as to produce large amounts of drag.

The presence of local flow curvature and the resulting virtual camber make foil profile optimization a challenge. However, inverse conformal mapping, as described in [7] (and used to generate Fig. 6) may be used to aid foil selection.

Preset Pitch Angle

Figures 7 and 8 show the turbine performance curves for two bladed and four bladed turbines (NACA0018) respectively. Several operational regimes are observed. At the highest preset pitch angles, the tip speed ratio drops below one, indicating a drag-based mode. A rise along a pre-stall tip speed ratio limit occurs for many of the sub-optimal preset pitch angles. The four bladed turbine exhibits a plateau at a high power coefficient for more optimal preset pitch angles, while the two bladed turbine stalls abruptly. Two factors may contribute to this phenomenon.

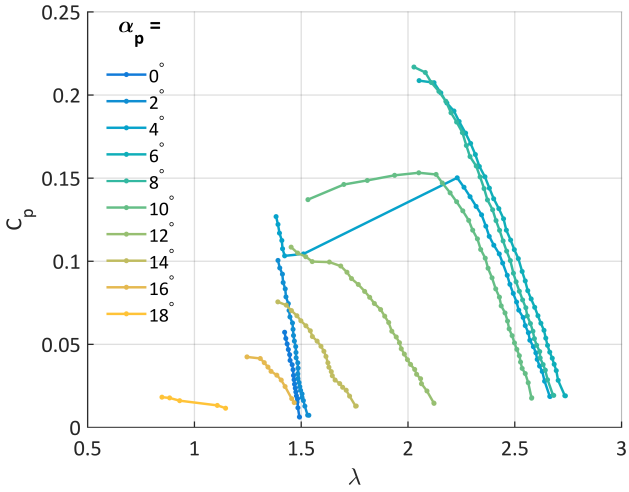

FIGURE 7: PERFORMANCE CURVES FOR $N = 2$ BLADED TURBINE AT VARIOUS PRESET PITCH ANGLES.

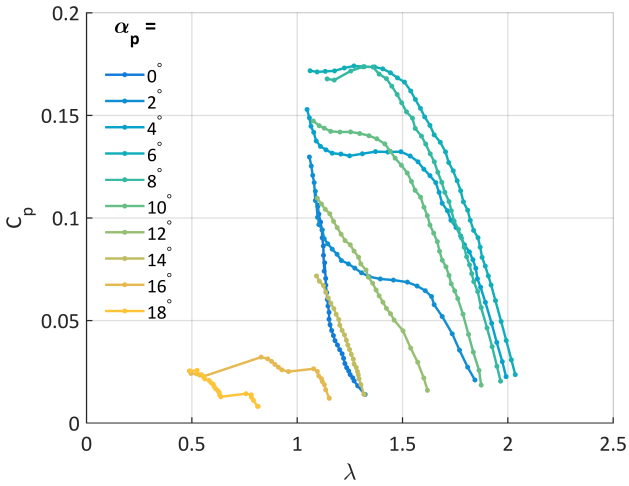

FIGURE 8: PERFORMANCE CURVES FOR $N = 4$ BLADED TURBINE AT VARIOUS PRESET PITCH ANGLES.

First, the cause of the plateau region for the four bladed turbine may be ascribed to virtual camber: As the resistive load is increased, tip speed ratio is slowly decreased. Because the virtual camber increases with decrease in tip speed ratio, it may start to increase drag on the device, thus halting further increase in performance. Second, the greater torque variation (and thus cyclical tip speed ratio variation) for the two bladed turbine may make it more prone to stall before reaching the plateau region.

For all turbines ($N = 1, 2$, and 4), the optimal preset pitch angle was found to be between 6-8 degrees (Fig. 9). As shown by Fig. 2, a positive preset pitch angle decreases the angle of attack during the upstream portion of the cycle, and increases it during the downstream portion. While an ideal turbine blade would extract as much energy from the flow during its upstream

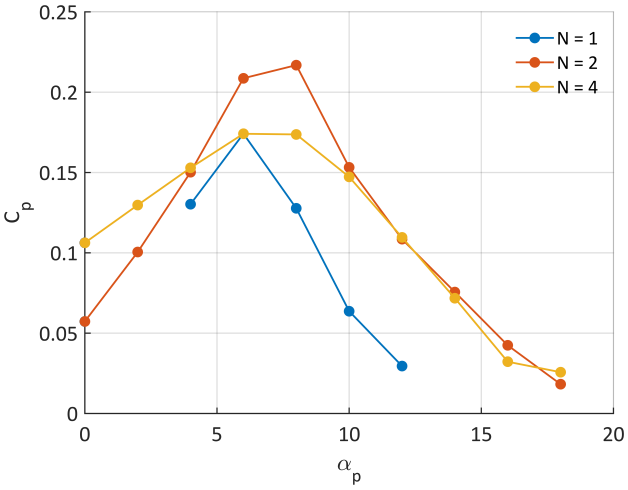

FIGURE 9: MAXIMUM POWER COEFFICIENT FOR EACH PRESET PITCH ANGLE.

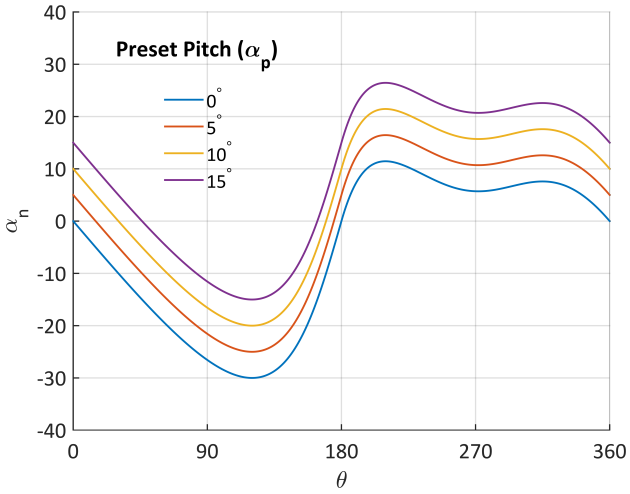

FIGURE 10: EFFECT OF PRESET PITCH ON THE NOMINAL ANGLE OF ATTACK AT THE MOUNT POINT ASSUMING A NEGATIVE COSINE WAKE DEFICIT (WITH A MINIMUM OF $0.2U_\infty$) FOR THE DOWNSTREAM PORTION OF THE BLADE TRAJECTORY, $\theta = 180 \rightarrow 360$. HERE $\lambda = 2$.

and downstream passes, due to the energy removed from the flow by the upstream blades, the apparent free stream velocity over the downstream pass is much lower. The effect of a free stream deficit on the nominal angle of attack is shown in Fig. 10. It is then apparent that adding a preset pitch angle helps to make the maximum nominal angle of attack equivalent during both halves of the cycle. During the upstream half (where adding preset pitch decreases the maximum angle), this may help avoid or delay blade stall. During the downstream portion, the angle of attack is increased to the optimal maximum.

The maximum performance was found with the two bladed turbine. The optimal number of blades is likely due to a balance of several factors. An increase in solidity reduces the maximum λ and more blades also likely generate more wake structures which subsequently interact with the blades over the downstream region. However, each blade produces some additional torque. In addition an increased number of blades results in less torque variation during the cycle, making the straight-bladed turbine less prone to stall.

CONCLUSIONS

We theorize that the effect of flow curvature (and thus virtual camber) plays a major role in determining the performance of foil cross section profiles and in the general operation of cross-flow turbines with high chord to radius ratios, especially at low tip speed ratios. In the case studied, a cambered foil performed worse than a symmetric one.

We find that preset blade pitch strongly influences performance at high chord to radius ratios. For a two bladed turbine we observed an increase in performance from $C_p = 0.057$ with zero preset pitch angle to $C_p = 0.217$ with a preset pitch angle of eight degrees. This massively outstrips the performance increase due to changes in preset pitch angle previously reported for lower chord to radius turbines. We also find a higher optimal preset pitch angle than previous studies [3] [4] [5].

In addition, we propose the importance of the internal wake deficit in the presented preset pitch results. A simple model suggests that the wake deficit decreases the nominal angle of attack over the downstream region. Preset pitch normalizes the nominal angle of attack during cycle by reducing α_n in the the upstream region and increasing α_n in the downstream region. Flow field analysis is necessary to accurately determine the wake deficit and the factors that influence it. In addition, the role of dynamic stall and coherent wake structures and the resulting foil-structure interactions needs to be examined for a more complete understanding of the hydrodynamics of cross-flow turbines.

ACKNOWLEDGMENT

We would like to thank Naval Facilities Engineering Command for funding this research.

Thanks are also given to the University of Washington's Department of Aeronautics and Astronautics and Fiona Spencer for use of their water flume.

REFERENCES

[1] Salter, S., 2012. "Are nearly all tidal stream turbine designs wrong?". In 4th International Conference on Ocean Engineering.

[2] Sheldahl, R. E., and Klimas, P. C., 1981. Aerodynamic characteristics of seven symmetrical airfoil sections through 180-degree angle of attack for use in aerodynamic analysis of vertical axis wind turbines. Tech. rep., Sandia National Labs., Albuquerque, NM (USA).

[3] Klimas, P. C., and Worstell, M. H., 1981. *Effects of blade preset pitch/offset on curved-blade Darrieus vertical axis wind turbine performance*. Sandia National Laboratories.

[4] Rawlings, G. W., 2008. "Parametric characterization of an experimental vertical axis hydro turbine".

[5] Fiedler, A. J., and Tullis, S., 2009. "Blade offset and pitch effects on a high solidity vertical axis wind turbine". *Wind engineering,* ***33***(3), pp. 237–246.

[6] Glauert, H., 1936. "Aerodynamic theory: a general review of progress under a grant of the guggenheim fund for the promotion of aeronautics".

[7] Migliore, P. G., Wolfe, W. P., and Walters, R., 1980. "The effects of flow curvature on the aerodynamics of darrieus wind turbines". *NASA STI/Recon Technical Report N,* ***81***, p. 15542.

[8] Armstrong, S., Fiedler, A., and Tullis, S., 2012. "Flow separation on a high reynolds number, high solidity vertical axis wind turbine with straight and canted blades and canted blades with fences". *Renewable Energy,* ***41***(0), pp. 13 – 22.

[9] Gosselin, R., Dumas, G., and Boudreau, M., 2013. "Parametric study of h-darrieus vertical-axis turbines using urans simulations". *21st Annual Conference of the CFD Society of Canada*.

[10] Consul, C. A., Willden, R. H., and McIntosh, S. C., 2013. "Blockage effects on the hydrodynamic performance of a marine cross-flow turbine". *Philosophical Transactions of the Royal Society A: Mathematical, Physical and Engineering Sciences,* ***371***(1985), p. 20120299.

[11] Niblick, A. L., 2012. "Experimental and analytical study of helical cross-flow turbines for a tidal micropower generation system". PhD thesis, University of Washington.